CAPILLARY DESATURATION CURVES AND INSIGHTS ON TRAPPED OIL AT THE PORE SCALE, IN WATER-WET AND OIL-WET SANDSTONES

Hélène Berthet, Prisca Andriamananjaona, Sandra Barbouteau, Mathilde Hebert, Remi Farwati, Redouane Meftah, Gerard Quenault, Jean-Philippe Chaulet, Regis Brugidou, and Richard Rivenq
TOTAL SA, Avenue Larribau 64018 Pau Cedex, France

This paper was prepared for presentation at the International Symposium of the Society of Core Analysts held in Trondheim, Norway, 27-30 August 2018

ABSTRACT

Capillary desaturation experiments are combined with high-resolution micro-tomography imaging to understand the impact of wettability on the global and local distribution of fluids in the pore space of sandstone outcrops. Small cylindrical rock samples are cored, imaged in dry state then successively prepared at irreducible water saturation before steps of waterflood. Several samples also go through a wettability alteration phase in order to expand the range of wettability conditions: namely, oil-wet to mixed-wet. Waterflooding is done at various capillary numbers and injected brine volumes, depending on the case. The entire rock is imaged at voxel resolutions of typically 2 or 4 micrometers, to ensure a high-quality segmentation.
Global oil saturation results show how the wettability impacts the shape of capillary desaturation curves, in particular the existence of a critical capillary number. In the non-water-wet experiments, oil saturation is controlled by a large, highly-connected oil cluster percolating from the inlet to the outlet of the sample. Such results are important for pore-scale flow modeling strategy and validation. We demonstrate that the wettability is not always uniformly distributed along the core despite of the use of classical wettability alteration protocols, highlighting potential biases in traditional SCAL tests.

INTRODUCTION

Experimental waterflooding on cores drained with reservoir oil have long been used by reservoir engineers, as a key tool to study the impact of capillary forces and viscous forces on the amount of oil that remains microscopically trapped in a well-swept porous medium [1,2]. This information is essential for the oil and gas industry to design efficient production processes as well as EOR techniques that will target mobilization of the trapped oil. Most of capillary desaturation studies were carried out on water-wet systems, though most of the oil fields are oil-wet to intermediate-wet. Capillary desaturation curves (CDC) used to represent the evolution of oil saturation with respect to the capillary number (balance of viscous and capillary forces) may greatly vary with the system wettability as recently suggested by [3,4]. Pore network characteristics (pore

geometry and mineralogy) also appear to have an impact on the shape of the capillary desaturation curves.
For strongly water-wet systems, the residual oil saturation S_{orw} remains constant in the lowermost range of capillary numbers up to a critical number above which oil starts to be mobilized with S_{orw} decreasing. For non-water-wet systems, experimental works reported in the literature show a more gradual change of oil saturation with increasing capillary number or critical values of these numbers significantly different from the strongly water-wet case ([3,4,5,6,7]).

CDC are the averaged results of local microscopic processes that take place at the pore scale. It is therefore very important to study the oil saturation in a more local manner. Experimental biases such as capillary-end-effects, preferential flow pathways, also need to be verified to ensure high experimental quality. One technique used by oil companies is to obtain saturation profiles using radiographies of the core during the waterflooding [8]. Recent advances in X-ray tomography can greatly help us characterize the trapping patterns with much higher precision, at the pore scale, at various stages of the capillary desaturation process ([9, 10,11,12]). This is achieved by visualizing the distribution of fluid phases within the pore space of a small core plug (typically a few mm wide and cm long) during stationary stages of a water-based flood. Similarly to what has been done in the past with respect to the macroscopic characterization of capillary desaturation curves, pore scale investigations using X-ray tomography focused first on strictly water–wet cases and only recently results were reported on non-water wet cases, without imaging the entire sample [13,14].

In this work, we carry out capillary desaturation experiments on sandstones at various wettability conditions combined with x-ray imaging in order to visualize and analyze the trapped oil phase within the pore structure. The entire rock sample is imaged at the end of each waterflood (static conditions) at micrometer voxel size to well resolve the pore structure. Sub-micron resolution imaging is also carried out to better see details of the distribution of fluids according to the wettability.
The water-wet test is an interesting case to start with in order to compare with literature results. We focus on three other experiments for which the rock wettability was altered towards an oil-wet system. Our analysis is based on the comparison between water-wet and oil-wet cases, from a macroscopic point of view (capillary desaturation curve) to local investigation of the trapped oil phase.

MATERIALS AND METHODS

We chose to work on Fontainebleau and Bentheimer sandstone outcrops as they have been widely used in petrophysics studies [12]. Their advantage also stands in their pore sizes that are large enough for a good quality x-ray imaging. Figure 1 shows region-of-interest tomographies on both rocks, at very high resolution done on TOTAL's micro-tomograph (ZEISS Versa 520T). The main mineralogy difference is the presence of clay in the Bentheimer rock.

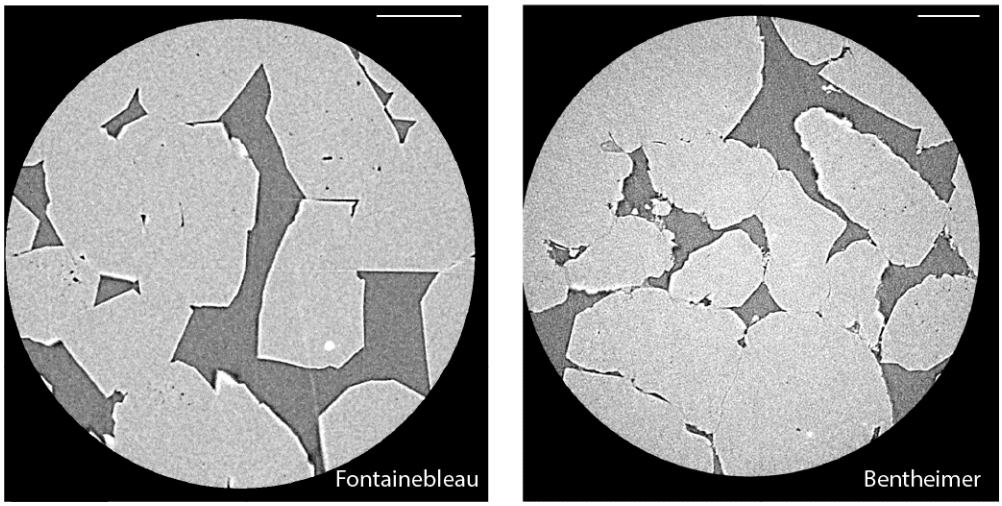

Figure 1: Images of our Fontainebleau (left) and Bentheimer (right) samples obtained from high resolution region-of-interest micro-tomography (image resolutions respectively 590 nm and 409 nm/voxel). Pores appear dark, grains appear bright. The scale bar indicates 100 µm.

For each experiment, a sample of approximately 4 mm in diameter and 30 mm in length is mounted in a microfluidic flow-cell developed at TOTAL. This apparatus constitutes a microfluidic Hassler cell that can be positioned on the sample stage of the micro-tomograph enabling high resolution 3D imaging as well as precisely-controlled microfluidic flow of oil or brine at high pressure and temperature (up to 100 bar, 100 °C). For the experiments described in this article, the operating conditions were: 20 bars of internal pressure, 40 bars confining pressure, 28°C temperature (temperature inside the micro-tomograph).
The wettability alteration is obtained by heating up the sample at 90°C for two weeks, following a recipe developed at TOTAL specific to the crude oil used. The temperature inside the flow cell is regulated, as well as the pressure of the oil phase, throughout the entire time. The flowcell is kept inside the micro-tomograph. A similar technique was applied in [3].

The cell is connected to a microfluidic flow circuit dimensioned for the precise flow of crude oil, brine and solvents in pressure and temperature (mainly computer-controlled syringe pumps, sensors, valves from CETONI, https://www.cetoni.de/). The flowrates used in these experiments ranged between 0.84 µL/min up to 5 mL/min. We also designed our flowcell so that we could control the flow circuit while continuously acquiring radiographs of the sample and the inlet/outlet tubings. We are therefore able to detect the arrival of brine just before it enters the sample in order to measure our dead volumes, then detect it as it flows out of the sample to obtain the brine breakthrough point.
Table 1 details the experimental conditions of each experiment analysed in this article. The capillary number (Ca) is computed with the injected fluid viscosity, flowrate and measured brine/decane or brine/crude oil interfacial tension: $Ca=\nu V/\gamma$.

EXPERIMENTAL PROCEDURE

The entire sample, mounted in the flow-cell, is first scanned dry at 2-µm voxel size. We then vacuum-saturate it with brine and drain it with oil until Swi is reached (irreducible water saturation) at a capillary number of 10^{-5}. See table 1 for details on the fluids used. The samples used for the oil-wet experiments are directly oil saturated (Swi=0) before going through the wettability change step. We then perform a series of successive waterfloods and scans of the entire sample. For the water-wet experiment, the waterfloods consist in injecting 1.5 pore volumes (PV) of brine, at increasing flowrates (capillary number). The oil-wet experiments differ as, for a given flowrate, we have several steps of brine injections, using increasing volumes of brine. Then the flowrate is increased, and we again flow at steps of brine volumes. For example, in the first oil-wet experiment, we successively injected 0.24 then 1 then 4 PV of brine, etc.

After each waterflood, we perform a series of tomography to capture the fluid distribution in the entire sample. The voxel resolution varies between 2 and 4 µm depending on the operational constraints. Over all, flooding steps are never longer than a few hours, accelerating to only tens of seconds for the highest flowrates. The scanning time is however of the order of 20 hours for a 4-µm voxel resolution image, reaching two days for a 2-µm voxel resolution scan. During this waiting time, the internal pressure of the flooding phase is regulated using the microfluidic flow system.

Rock	Porosity	Wettability	Swi	Waterflood steps	Oil	Brine
Fontainebleau	17%	water-wet	18%	1,5PV injected at each flowrate	decane	Water+NaI
Bentheimer *Experiment 1*	22%	oil-wet	0	flowrate fixed (Ca=10^{-7}), steps of brine injections	crude oil	Water+NaCl+CaCl2+KI
Bentheimer *Experiment 2*	22%	oil-wet	0	Steps of brine injection + flowrate steps	crude oil	Water+NaCl+CaCl2+KI
Bentheimer *Experiment 3*	22%	oil-wet	0	Steps of brine injection + flowrate steps	crude oil	Water+NaCl+CaCl2+KI

Table 1 Experimental conditions for the water-wet and the three oil-wet experiments

IMAGE PROCESSING

The processing of each scan follows a multi-step workflow (see Figure 2) and is done using TOTAL's supercomputer and ANU's image processing software MANGO (https://physics.anu.edu.au/appmaths/capabilities/mango.php). The region of interest is extracted from the raw data (3D reconstructed volume) to mask the sleeve around the sample and the inlet and outlet tubings. We optimize the masking so that the sample volume is almost entirely kept in the processed image.

We then filter and segment each dataset into two or three phases: oil, brine and grains, using a region-growing segmentation method from ANU [15]. Global saturations and saturation profiles are obtained from the segmented images. In order to study the pore-space fluid occupancy and the fluids connectivity, we perform a partitioning step of the

pore space to identify individual pores, and a partitioning of the oil phase to identify disconnected oil clusters.

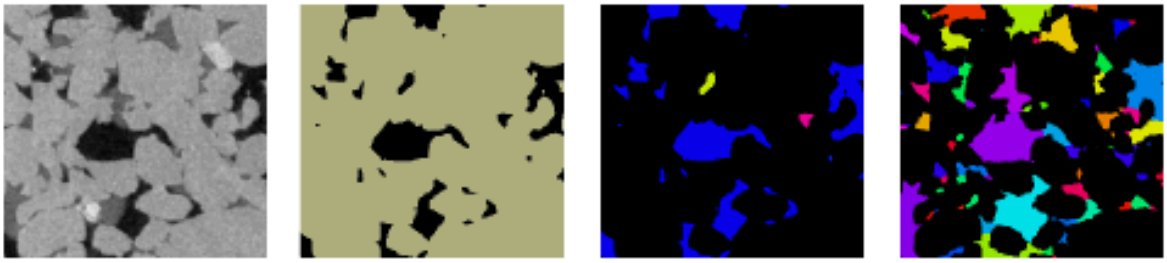

Figure 2: Processing workflow from the raw 3D image to local analysis of fluids distribution in the pore space. The third panel shows only the oil voxels in the image, color-coding each connected ganglion of oil. Similarly, each individual pore is assigned a given label (color) in the pore-space partitioning phase based on geometrical analysis (right-end panel).

RESULTS

Evolution of the oil saturation, at the sample level

Our first experiment, in water-wet conditions, constitutes a unique dataset at the pore scale level, as seven steps of waterfloods were realised and fully imaged at a voxel resolution of 2 µm. Figure 3 shows the evolution of the global oil saturation with respect to the capillary number. Oil saturation is simply obtained by counting the voxels assigned to the oil phase during the segmentation step of the processing. We normalised the S_{or} value by the S_{or*} (=38%), saturation obtained after the first waterflood. The agreement with the literature is excellent: plateau of saturation before a critical capillary number of 3.10^{-5}.

Oil saturation profiles along the sample length are interesting illustrations of the complexity of the untrapping and trapping of oil at the pore scale. Figure 4 shows three profiles, one at the end of the saturation plateau (blue), and two as the oil saturation significantly decreases. The smoothed curves were obtained in two steps. First we computed the porosity Representative Elementary Volume [13] from the dry image: 3 mm^3. Then we smoothed the saturation profiles with a moving average using a distance equal to the REV divided by the sample surface area. Imaging the entire sample enables to detect if some regions of the rock are affected by boundary effects, and if saturations should be computed in a restricted volume only.

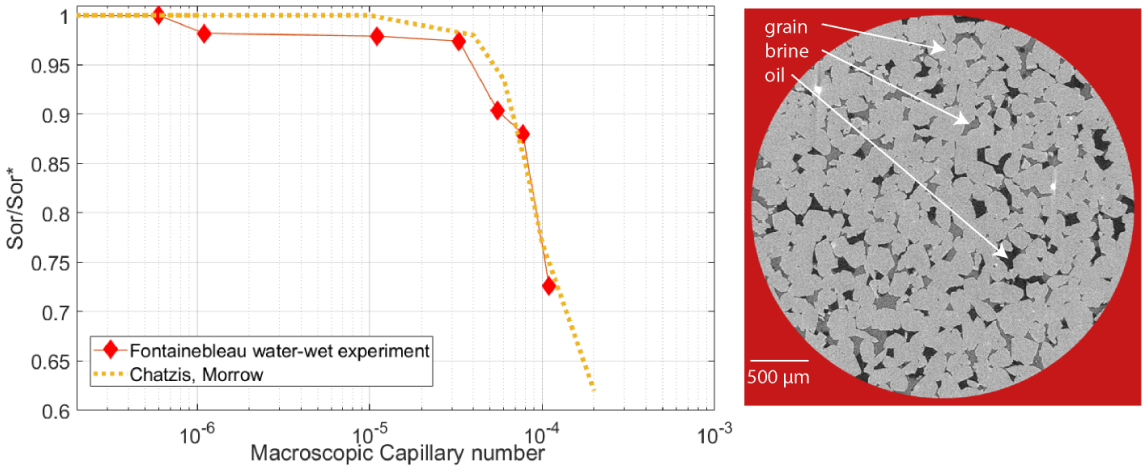

Figure 3 Capillary desaturation curves for the water-wet Fontainebleau experiment, compared to Chatzis and Morrow [1]. Oil saturation is normalised by saturation after the first waterflood. Right: section of the imaged volume at Swi (82%), corresponding to the entire sample diameter (2µm/voxel).

Figure 4 also shows an image from the reconstructed volume extracted in the middle plane, as well as a zoom on a few pores to illustrate the local distribution of oil and brine: the curvature of the oil/brine interface clearly indicates a water-wet system. This image also shows that the trapped oil can be disconnected in drops in the pore matrix.

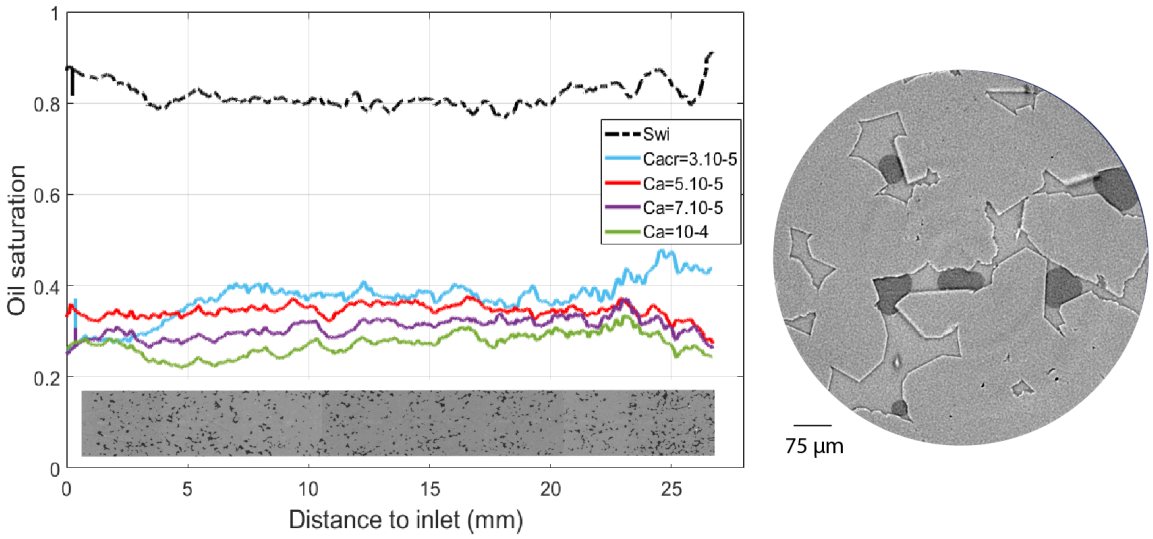

Figure 4 Evolution of the oil saturation along the sample length. The bottom image shows an image extracted in the middle plane of the sample. The right-side image shows the local distribution of fluids, in a water-wet case obtained by imaging at 800 nm/voxel.

We now focus on the first oil-wet experiment with a macroscopic view of the oil saturation evolution, with respect to the injected brine volume (Figure 5). Oil recovery

increases rapidly at start of the waterflood (though less than in the water-wet case), with 40% of the oil mobilised in less than 2 PV injected. As we continue injecting, the oil saturation continues to drop but much more slowly, without any sign of stabilization. This slower regime could correspond to the thinning of oil layers along the grains which are visible on the image of figure 5. Note also the curvature of the brine-oil interface and the presence of brine droplets in pores, illustrating that the sample is oil-wet.

The capillary desaturation curves of the oil-wet experiments are presented in Figure 6. The different data points for a given capillary number correspond to the several injections at increasing volumes of brine. The graph should therefore be read from left to right and top to bottom when applicable. In the third experiment, we were able to detect the breakthrough point (second data point of the graph). The saturation computed numerically (voxel count) compared very well with the injected brine volume.

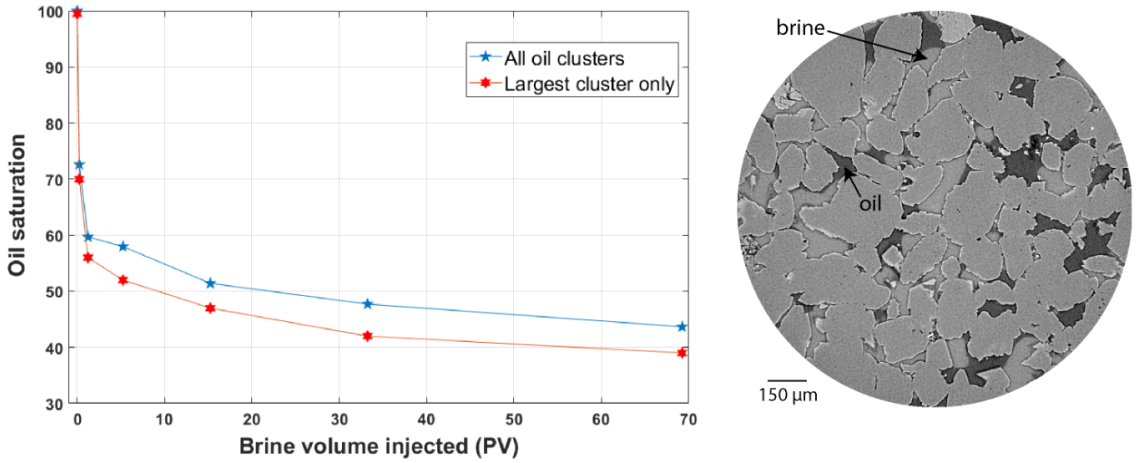

Figure 5 Evolution of oil saturation with respect to the injected brine volume, in the first oil-wet experiment. The right-side image was obtained from a scan of the sample after the last waterflood, at 800 nm/voxel resolution.

The second experiment displays a continuous decrease without a critical capillary number. In the third test, the oil saturation steadily decreases until it stabilizes when $Ca=10^{-5}$ to 10^{-4} before a significant drop down to 20%. Note on the inset of figure 6 that we reach very large quantities of injected brine due to the successive waterfloods.

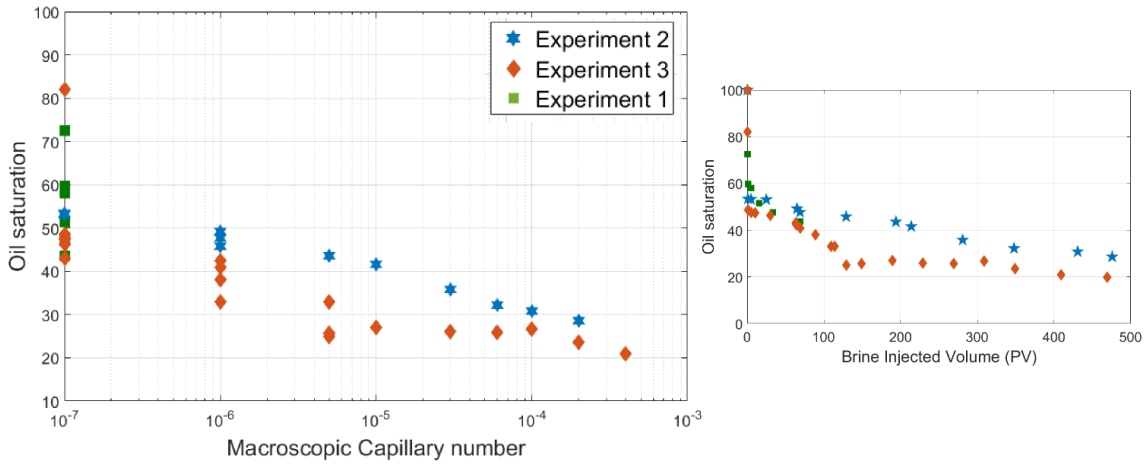

Figure 6 Capillary desaturation curves for the oil-wet experiments (Bentheimer rock). Inset: oil saturation versus the cumulative volume of injected brine.

Though similar wettability change techniques were used between the three experiments, the recovery is much higher for the third test: 28% at $Ca=10^{-5}$ compared to just above 40% in the second test.

Connectivity of the oil phase

We now focus on the connectivity of the oil phase by processing the segmented data further. Two oil voxels are considered connected if they are in contact through faces, vertices, or edges (26 degrees of connectivity). In figure 7, we visualize the oil connectivity by looking only at the oil phase and color-labelling each independent oil cluster. Three steps of the water-wet Fontainebleau experiment and the first oil-wet experiment are illustrated. In the Fontainebleau test, we observe a lot of oil fragmentation due to snap off events in the constrictions of the pore space [16]. From the first waterflood (<1 PV injected) to the fourth one (at the critical capillary number), the 18000 blobs of oil fragment into 59000 clusters. The largest blob corresponds to 0.3 % of the oil in place. In the first oil wet experiment, represented in the lower row, the oil stays highly connected within a cluster percolating from the inlet to the outlet of the core. Note also the shape of the oil blobs: for the water-wet rock, oil blobs have rounded borders as they are surrounded by brine in the pores. In the second case, the oil is in contact with the grains, giving them rougher borders.

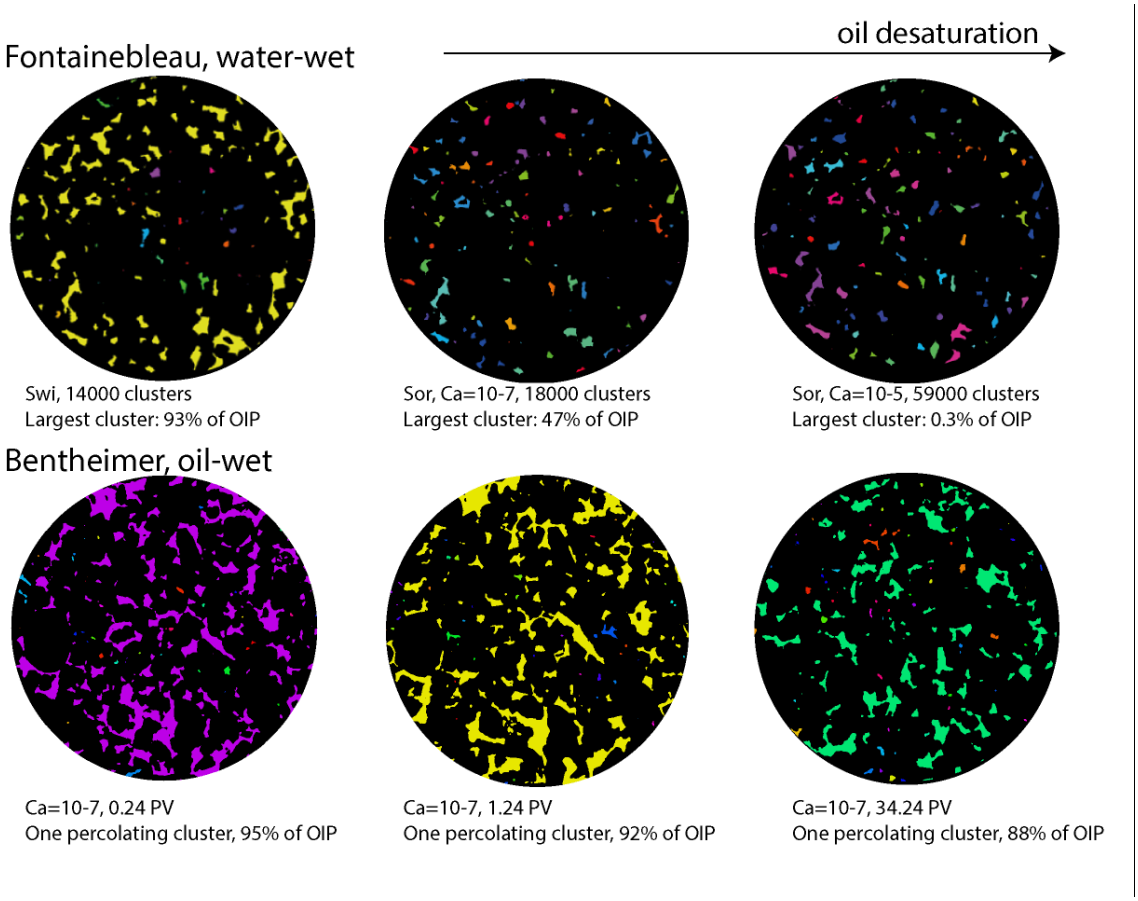

Figure 7 Evolution of the connectivity of the oil phase depending on the wettability and the rock. The same slice extracted from the imaged volume is displayed after each waterflood. Brine and grain voxels are black. Each group of connected oil voxels, constituting an oil blob, is identified by a colored label. In the water-wet case, oil gets more and more disconnected, contrary to the oil-wet case. OIP=oil in place.

As shown in Figure 7, it is interesting to follow the proportion of oil contained in the largest oil cluster for all desaturation experiments. Its evolution, waterflood after waterflood and for the four experiments is plotted in figure 8.Three trends can be observed. When the rock is water-wet, talking about a largest cluster is meaningless as it only counts for a few percent of the trapped oil, after the second waterflood. On the contrary, in the oil-wet experiments the largest cluster, after six waterfloods, still contains more than 80% of the remaining oil in place (see also Figure 4). An intermediate behavior is found for the two other oil-wet experiments. We observe a large connected cluster at the beginning of the desaturation that gets fragmented into clusters counting for a few percent of the oil in place. As explained before, we maximize our chances of considering two voxels connected as we take into account contact between vertices. Nevertheless, noisy images and resolution limit could lead to disconnected segmented voxels that are actually connecting. We looked at the second biggest cluster present in the second oil-wet experiment. The only significant change is obtained for the data point at

229 PV as seen on the inset of Figure 8. We can therefore confirm the change of regime towards a more fragmented trapped oil.

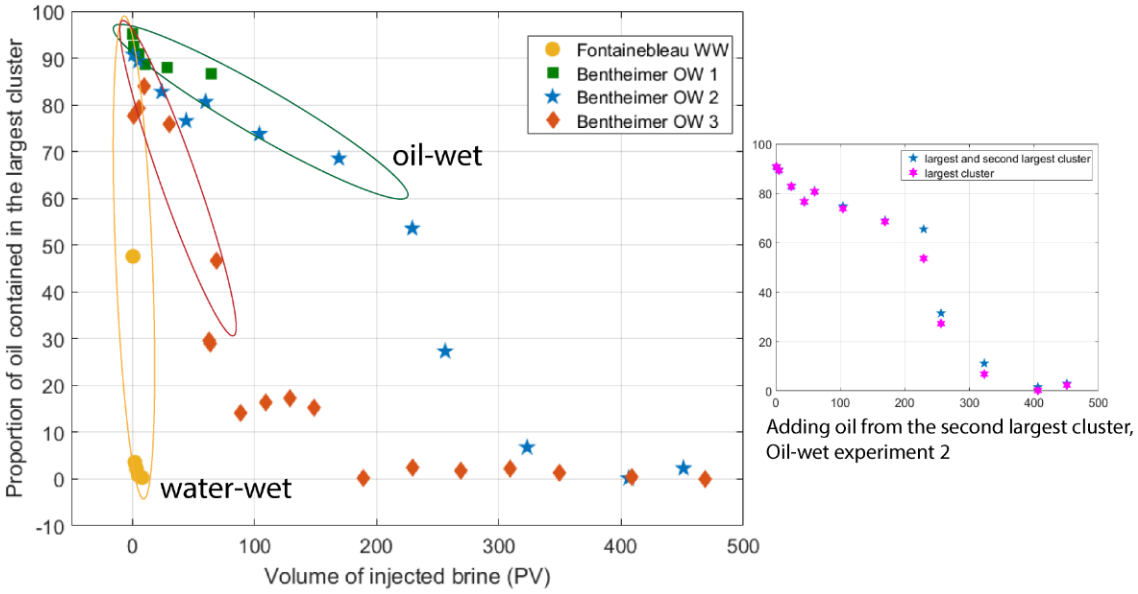

Figure 8 Oil contained in the largest oil cluster present after each waterflood step, in percentage. WW: water-wet, OW: oil-wet.

The critical behaviour of the largest cluster size occurs at macroscopic capillary numbers of 10^{-7} in the water-wet experiment, 10^{-6} in the third oil-wet experiment, and 10^{-5} in the second oil-wet experiment.

Oil-wet experiments 1, 2 and 3 were all performed using the same wettability change protocol. We confirmed the wettability change, as explained earlier, by tracking the curvature sign of the oil/brine interface. However the differences observed between the three CDC as well as the differences in connectivity behaviour led us to revisit the "raw" data: the imaged volumes. We navigated through the thousands of images waterflood by waterflood and were able to find images in which the distribution of fluids changes completely from a pore to the next one, as illustrated in Figure 9. Curvature of the oil/brine interface changes sign at very small distance. We couldn't find similar images in the first oil-wet experiment, which we consider more uniformly oil-wet. It is also worth noting that these results are not due to a change of wettability over time though large quantities of brine were injected, during long experiments. An automatic contact angle measurement tool would be useful to quantify the wettability heterogeneity in terms of location and difference in angle value, to explain why the recovery of the third experiment is better despite an earlier loss of connectivity of the oil phase.

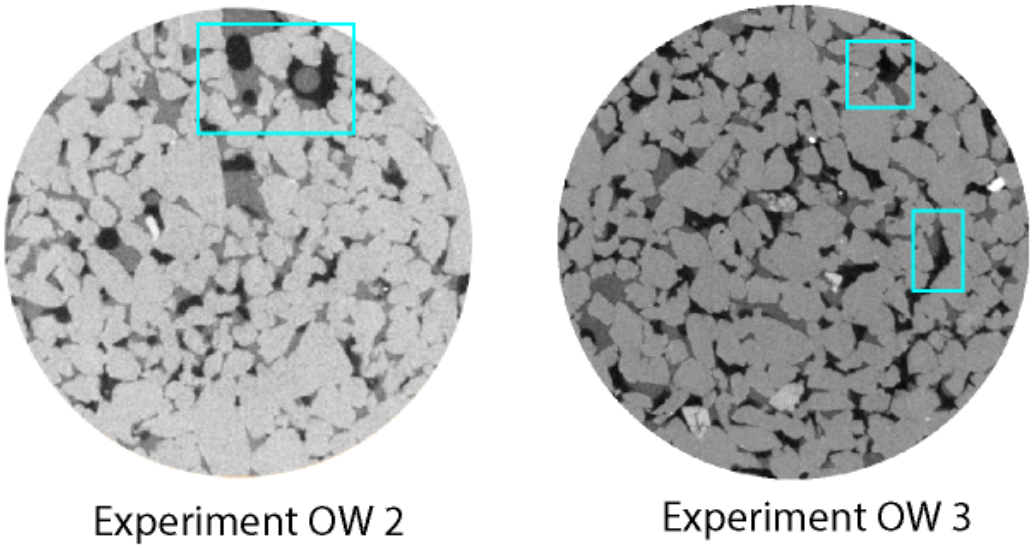

Figure 9 Slices extracted from oil-wet experiments 2 and 3 in which the curvature of oil blobs changes sign from one pore to the next. Similarly, oil can be seen in the middle of a pore, surrounded by brine (water-wet like), as well as along pore grains (oil-wet like).

CONCLUSION

In this work, a series of capillary desaturation experiments was conducted on sandstone outcrops and combined with x-ray microtomography imaging of the entire rock samples to capture the distribution of oil and brine in each pore, at each waterflood step. Wettability was altered from water-wet towards oil-wet by leaving the sample saturated with reservoir oil, at high temperature for two weeks. One sample was left water-wet. A detailed analysis of the trapped oil phase and through its connectivity highlights large differences of fluid behavior depending on the wettability. In oil-wet experiments, the trapped oil remains highly connected, and loss of connectivity seems to be a clear indicator of water-wettability. Differences between all three oil-wet desaturation experiments show the difficulty to reproduce experiments involving wettability changes. We also demonstrate that traditional wettability-change methods may not lead to a homogeneous change everywhere in the pore space. All the highlighted microscopic signatures of wettability lead to capillary desaturation curves that greatly vary between water-wet and oil-wet sandstones. Quantitative measurements of contact angles, at the pore scale, will be very useful to further detail our analysis of these unique datasets, in particular to understand the heterogeneous distribution of wettability.

REFERENCES

1. Chatzis, I., Morrow, N. R. “Correlation of Capillary Number Relationships for Sandstone”. *Society of Petroleum Engineers (1984)*, 24, 555-563

2. Chatzis, I., Kuntamukkula, M. S. and Morrow, N. R. “Effect of capillary number on the microstructure of residual oil in strongly water-wet sandstones”. *Society of Petroleum Engineers Journal (1988), 3(3):902–912.*
3. Humphry, K. J., Suijkerbuijk, B. M. J. M., van der Linde, H. A., Pieterse, S. G. J. and Masalmeh, S. K. “Impact of Wettability on Residual Oil Saturation and Capillary Desaturation Curves”. *Society of Petrophysicists and Well-Log Analysts*, 2014, 55.
4. Masalmeh, S. “Impact of Capillary Forces on Residual Oil Saturation and Flooding Experiments for Mixed to Oil-Wet Carbonate Reservoirs”, *Proceedings, SCA International Symposium (2012)*
5. Jadhunandan, P. P., Morrow, N. R.” Effect of Wettability on Waterflood Recovery for Crude-Oil/Brine/Rock Systems”. *Society of Petroleum E*ngineers (1995), 10.
6. Morrow, N., Chatzis, I., Taber J. “Entrapment and mobilization of residual oil in Bead Packs”. *SPE Reservoir Engineering Journal (1988),* 927-934
7. Mohanty, K., Salter, S. “Multiphase Flow in Porous Media: III. Oil Mobilization, Transverse Dispersion and Wettability”, *Society of Petroleum Engineers (1983),* 12127
8. Puyou,G., N’Guyen M., Savin, S., « CXBOX : An Innovative Tool For Fluid Dynamic Quantification During Corefloods », *Proceedings, SCA International Symposium 2017*
9. Wildenschild, D., Sheppard, A.P. “X-ray imaging and analysis techniques for quantifying pore-scale structure and processes in subsurface porous medium systems”. *Advances in Water Resources (2013)*, 51, 217-246.
10. Youssef, Y., Peysson, Y., Bauer, D., Vizika, O. “Capillary desaturation curve prediction using 3D microtomography images”, *Proceedings, SCA International Symposium 2015-008*
11. Armstrong, R.T., Georgiadis, A., Ott, H., Klemin, D. and Berg, S. “Critical capillary number: Desaturation studied with fast X-ray computed microtomography”, *Geophysical Research Letters (2015)*, 41, 55-60
12. Oughanem, R., Youssef, S, Bauer, D., Peysson, Y., Maire, E., Vizika, O. “A Multi-Scale Investigation of Pore Structure Impact on the Mobilization of Trapped Oil by Surfactant Injection”, *Transport in Porous Media (2015),**109,** 3, 673*
13. Singh, K., Bijeljic, B., Blunt, M. J. “Imaging of oil layers, curvature and contact angle in a mixed-wet and a water-wet carbonate rock” *Water Resources Research* (2016), 52, 3, 1716-1728
14. Blunt, M.J. “Multiphase flow in permeable media: a pore-scale perspective” Cambridge University Press, Cambridge, 2017
15. Sheppard, A.P., Sok, R.M., Averdunk, H [2004] Techniques for image enhancement and segmentation of tomographic images of porous materials. *Physica A*, 339, 145-151.
16. Roof, J. G. [1970] Snap-Off of Oil Droplets in Water-Wet Pores. *Society of Petroleum Engineers*, 10, 85-94